공학석사 학위논문

Ion channel as an origin of inductance in perovskite solar cell

페로브스카이트 태양전지 내부 이온채널에 기인한 인덕턴스

2019 년 8 월

서울대학교 대학원

기계항공공학부

정 기 완

Ion channel as an origin of inductance in perovskite solar cell

Kiwan Jeong

School of Mechanical and Aerospace Engineering

The Graduate School

Seoul National University

Abstract

Physical inductance as an origin of inductive-loop (or negative cap) in perovskite solar cell is proposed. Light/bias induced inductive loop, abnormal transient response and inverted hysteresis were put together as consequence of light/bias induced inductance. Non uniform current density due to ion channel is suggested as an origin of inductance, and presence of ion channel in inverted hysteresis device were shown by HRTEM and EDS.

Keywords:

Perovskite solar cell **Inverted hysteresis** **inductive loop**

negative cap **ion channel**

Student Number: 2017-22307

Index

List of Figures

and e)0.8V. Step voltage for transient response analysis were all 0.1V.

Figure2.1.3 Bode plot of a) normal hysteresis and b) inverted hysteresis device for DC bias of 0.6V, 0.8V and 1.0V. c) Magnified Bode plot in linear scale of inverted hysteresis device under 1.0V DC bias.

Figure3.1.1 Change in JV curve under a) short circuit case and b) open circuit case and then dark recover. RS/FS refers to reverse/forward scan. c) Result of periodic alternative bias voltage (1.2V, -0.2V. 1hour for each step) in terms of hysteresis index.

Figure3.1.2 High-resolution TEM image of (a) normal hysteresis device and (b) inverted hysteresis device. Corresponding EDS mapping of iodide atom (L series) of (c) normal hysteresis device and (d) inverted hysteresis device. (e) Fast Fourier transformed micrograph of marked region in (b). Scale bar present in each figure.

Figure3.1.3 Schematic for explanation how non uniform current density can behave as inductance. Two different current I_1, I_2, length, distance, radius of current path d, s, R, bias voltage V and magnetic permeability μ are shown. Parameter r is ratio of two current I_1 and I_2.

Chapter 1. Introduction

1.1. Study background: Principle of solar cell device

1.1.1. Band structure and device structure

Unlike classical mechanics, not all energy level for bound state is available in quantum mechanics. This is due to wave-particle duality of extremely small particle such as electron bounded to atom. Discretized energy spectrum disperses as another atom is put nearby. As the number of adjacent atoms grows up, this dispersion becomes larger with its width limited. As a result, electrons bounded to material with size that human can observe without any equipment, almost consists of $6.02*10^{23}$(Avogadro number) atoms, form semi-continuous energy band. This is called band structure. Electrical insulator is material without overlap of conduction band and valence band. But even in that case, with enough energy to excite electron from valence band to conduction band, insulator can conditionally be conductive. For example, light with enough energy excites electron in valence band to conduction band, leaving hole in valence band as the light is absorbed. Minimum energy for such excitation is called band gap energy, and is mathematically difference between conduction band edge and valence band edge. Semiconductor is material with this quantity small enough to be controlled by human technology (less than 2eV) (Fig.1.1.1a). Study of quantum mechanics and band theory are fruitful for deeper understanding.

When different materials are put closely, each band structure aligns to each other as a consequence of charge transfer by diffusion mechanism. Here, band smoothening region is called junction(Fig.1.1.1b). Due to transferred charge, gradient of electrical potential is present in the region, leading to charge extraction for excited carrier due to electric field (drift mechanism) (electron & hole) (Fig.1.1.1c) and nonlinear diode behavior with specific type of junction for charge injection(Fig.1.1.1d). Study of solid state physics, electrodynamics, statistical mechanics and semiconductor device physics are fruitful for deeper understanding.

Solar cell device, also called as photovoltaic device, consists of absorber layer and extraction layer. Device structure of device dealt in this paper have structure of thin absorber layer between electron transport layer and hole transport layer, forming two junctions at each side targeting different type of carrier (electron and hole, respectively) (Fig.1.1.1e).

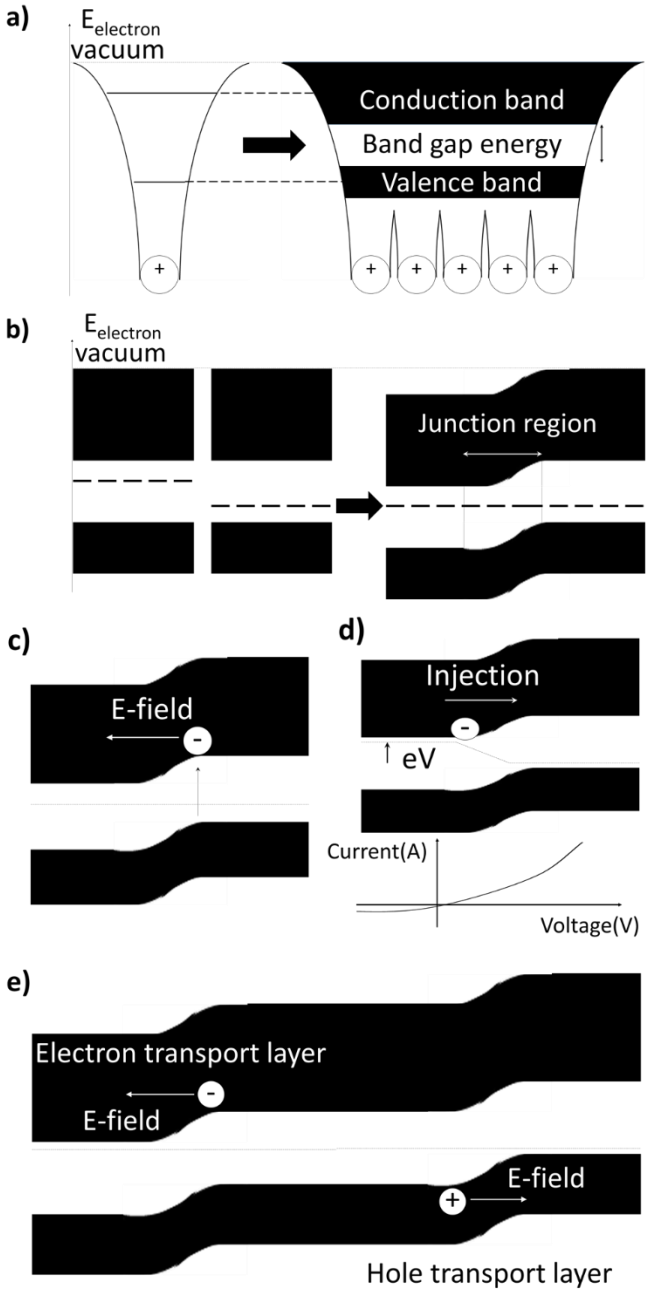

Figure1.1.1 Schematic explanation of a) band structure, b) junction, c) charge extraction, d) charge injection and e) device structure.

1.1.2 Carrier dynamics and equivalent circuit

Not all generated electrons and holes are extracted. They recombine with each other or get trapped to defect site. Only remaining carriers get extracted to each transporting layer. Extracted carriers return to the other end through external circuit, doing electrical work for load in external circuit. Even extracted carriers lose energy due to electrical resistance(Fig1.1.2a).

For study purpose, equivalent circuit can be constructed to depict these dynamics. Generation of carrier is put as current source, recombination is put as internally closed shunting circuit with shunt resistance(R_{sh}), injection of carrier due to biasing is put to diode, and energy loss due to electrical resistance is put as series resistance(R_s). Trapping of carriers can be put as capacitance, though effect of the capacitance is negligible for conventional inorganic solar cell(Fig1.1.2b).

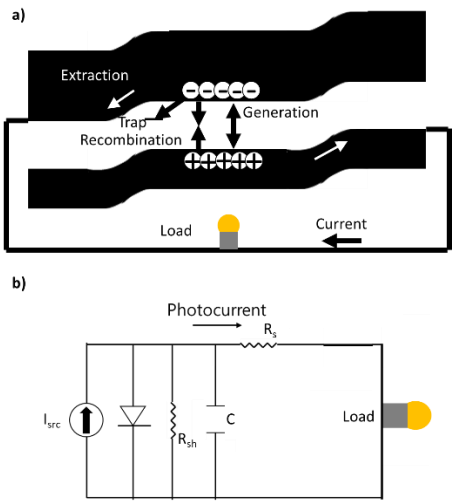

Figure1.1.2 Schematic explanation of a) carrier dynamics and b) equivalent circuit (R_s=series resistance, R_{sh}=shunt resistance and C=capacitance).

1.1.3 Photovoltaic parameters and measurement

When characterizing solar cell in laboratory, electrical load in external circuit is replaced to bias voltage opposing to photocurrent. For photocurrent generation, one can use solar simulator to describe sun experimentally. For energy harvesting purpose, current should flow opposite to bias voltage. Here, what matter is both load voltage and current since it is matter of power. Thus, characterization is done by measuring how much current flows for whole bias voltage in range of interest, by sweeping voltage. Linear staircase voltammetry sweep is often used for voltage sweep, where voltage profile is of step function. This is called IV scan, and the resulting curve is called IV curve. Voltage sweep with direction from opposing bias (forward bias) to assisting bias (reverse bias) is called reverse scan (RS), and sweep with opposite direction is called forward scan (FS). For purpose of fair comparison, current density per unit area is often used instead of current itself. In that case, those measurement and curve are called as JV scan and JV curve(Fig1.1.3a).

General JV curve is given in Fig.1.1.3b. Current (density) for zero load voltage (short circuit) is called short circuit current (density) (I_{sc}(J_{sc})), load voltage for zero current flow (open circuit) is called open circuit voltage (V_{oc}). Load voltage where the solar cell harvests power(density) the most is called maximum power voltage (V_{MP}), and corresponding current density is called maximum power current(density)(I_{MP}(J_{MP})). Efficiency is calculated by dividing this maximum power into sun power, and is called photo conversion efficiency(PCE). Ratio between maximum power and V_{oc}*J_{sc} is called fill factor(FF), and resistance(dV/dI) at short circuit case and open

circuit case is mathematically same as shunt resistance(R_{sh}) and series resistance(R_s) in equivalent circuit we discussed in previous section.

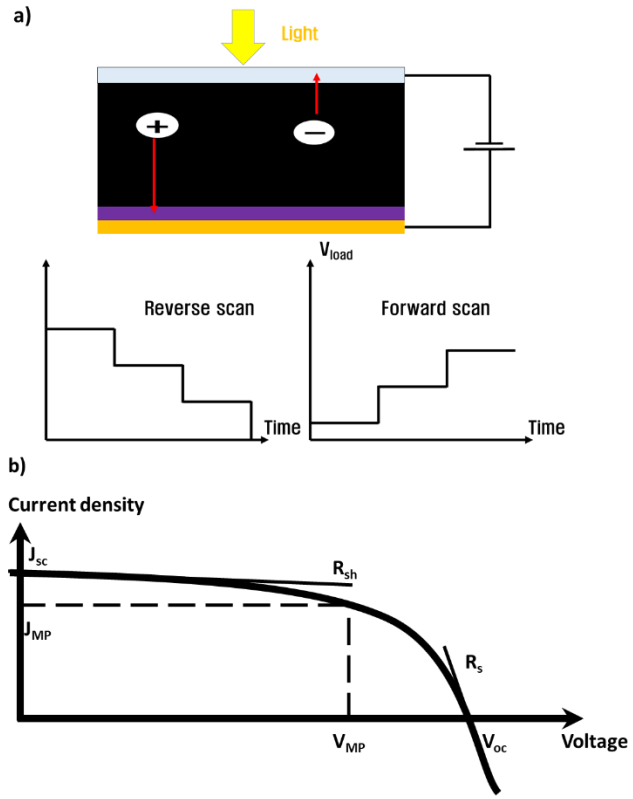

Figure1.1.3 Schematic explanation of a) voltage sweep and b) photovoltaic parameters in JV curve.

1.2 Study background: Perovskite solar cell

1.2.1 Perovskite material and its application

Perovskite material refers to material with specific crystal structure [1]. Any material with variety combination of different A(organic cation), B(metal cation) and X(halide anion) having this ABX_3 crystal structure are all referred by the terminology. This is also referred as organic(A)-inorganic(B) halide(X) perovskite(OIHP) to emphasize its hybridity of organic-inorganic material.

OIHP has been regarded as promising photovoltaic material for its superior optoelectronic properties and low price. As a result, from 2009 to 2019, photo-conversion-efficient (PCE) of perovskite solar cell (PSC) has grown from 3.81% to 22.7% in 10 years[1-7].

Its application was not limited to photovoltaics: light emitting diode (LED)[8, 9], field effect transistor (FET)[10], photo detector[11] and resistive random access memory (RRAM) device application[12, 13] has been reported. But still, as a light-absorbing layer in photovoltaic device, several topics about its working principle has not been fully elucidated.

1.2.2 Normal hysteresis and measurement

Hysteresis refers to every phenomenon where observation result is significantly affected by the path followed by the observation. Unlike conventional photovoltaic device, hysteresis in JV curve has been reported in PSC. Since first report of existence of hysteresis in OIHP photovoltaic device, study about physical origin of such hysteresis has been conducted[14-26].

Normal hysteresis (NH) is one type of hysteresis where magnitude of photocurrent for reverse scan is higher than that of forward scan (Fig1.2.2a). It is explained by not neglecting capacitance in equivalent circuit. Transient response analysis in time domain (JT curve) shows mono decreasing photocurrent in reverse scan and mono-increasing photocurrent in forward scan toward steady state current, due to charging/discharging of capacitance. Referred as normal transient response (Normal TR), this can explain normal hysteresis(Fig1.2.2b). Capacitive mechanisms other than trapping have been suggested, regarding essence of capacitance as delaying phenomenon. Ionic motion[20-24], ferroelectric effects[25] and unbalanced electron and hole fluxes[26] has been proposed as such delayed response phenomenon.

Since capacitance delays the signal, electrochemical impedance spectroscopy(EIS) where frequency response of PSC can be measured has been widely studied[14-18, 27, 28]. EIS measurement gives information about complex impedance, having information about amplitude and phase compared to input perturbation with single frequency for chosen DC bias

(Fig.1.2.2c). Dealing with sinosuidal signal using Euler equation($\mathbf{e^{i\theta} = \cos\theta + i\sin\theta}$), complex impedance is obtained. The data can be interpreted in both Bode plot and Nyquist plot. Bode plot expresses norm and phase of complex impedance according to frequency, and Nyquist plot expresses imaginary part according to real part of complex impedance, with imaginary part inverted. For simple RC circuit, norm of impedance decreases as frequency gets higher in Bode plot (Fig.1.2.2d). In Nyquist plot, distance from origin gets decreased as frequency gets higher, following half circle in(Fig.1.2.2e).

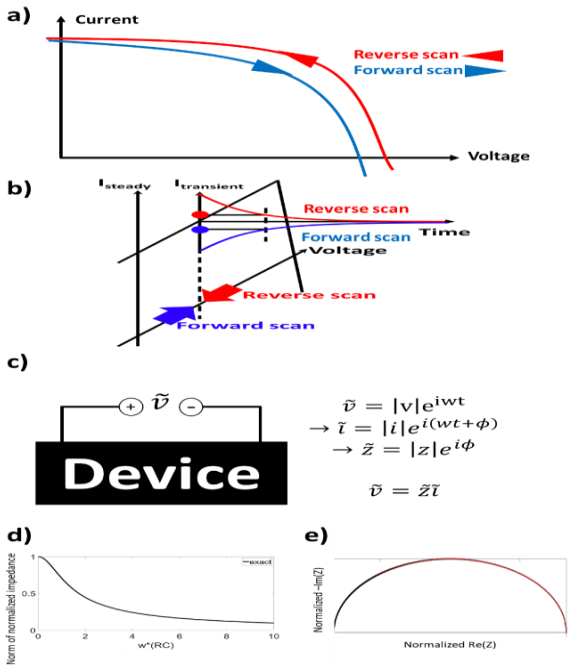

Figure1.2.2 Schematic explanation of normal hysteresis in a) JV curve, b) JT curve, c) Electrochemical impedance spectroscopy(EIS), d) Bode plot and e) Nyquist plot of EIS data for simple RC circuit.

1.2.3 Unexplained: Inverted hysteresis and inductive loop

While normal hysteresis in JV/JT curve and half circle in EIS data has been widely reported and well explained by introducing capacitance, several exceptional data have also been reported. Inverted hysteresis in JV curve and inductive loop-or negative cap-in EIS data are those. Inverted hysteresis is hysteresis in JV curve with more photocurrent in forward scan[15, 29-33](Fig.1.2.3a). Inductive loop in Nyquist plot for EIS data is same as maxima in Bode plot[14-18](Fig.1.2.3c, d). All those are explained by introducing inductance parallel to shunt path(Fig.1.2.3.b)– or at least dynamics with same mathematical form with that of inductance- since what it does is opposite to what capacitance does, by forming induced electromotive force [15, 16, 18, 34]**.** But, though suggestion regarding slow responding ionic accumulation induced recombination or barrier were made[16-18], physical origins of such inductive behavior are not yet identified.

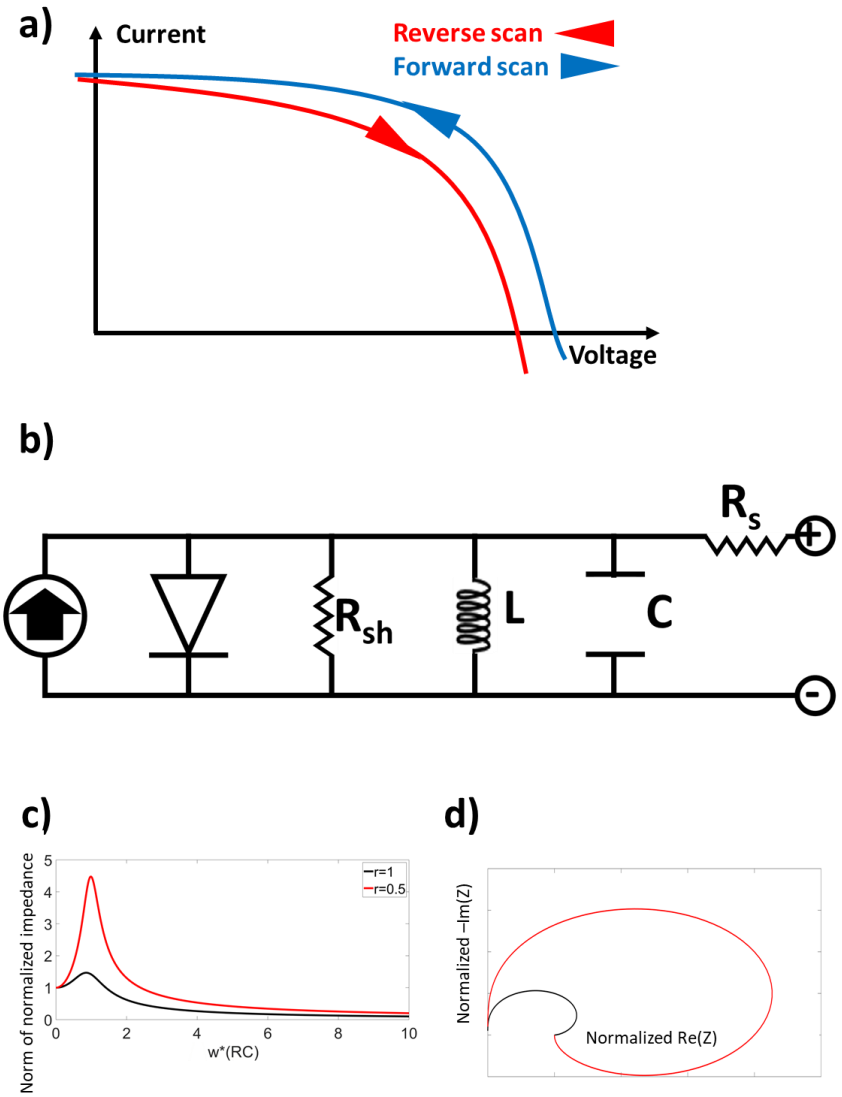

Figure1.2.3 Schematic explanation of a) Inverted hysteresis in JV curve, b) equivalent circuit with additional inductance and c) Bode plot and d) Nyquist plot of EIS data for depicted RLC circuit for different level of resistance (small r corresponds smaller resistance level).

1.3 Purpose of research

Regardless of fast evolution of PSC in terms of PCE, stability pr oblem is remaining, with mechanism of degradation has not yet been el ucidated. Since hysteresis reveals physical characteristics of the device, one can indirectly imagine change of dynamics in device via hysteresis. This type of approach is already present, meaning this method is reaso nable[35].

Purpose of this research is to find out the mechanism of PCE dro p via analysis of hysteresis. Specifically, the hysteresis dealt in this pap er is inverted hysteresis which is not present in initially. With various measurement more than just JV scan which is basic measurement for stability test, we can obtain information of the physical origin for such hysteresis.

Final goal is more than just academic understanding: it is to sugg est useful agenda for stability problem. If one solves the problem based on suggested agenda, it would be great honor.

Chapter 2.

Light/bias induced inductive behavior

2.1. Results and discussion

2.1.1. Change in JV curve

Glass/ITO/SnO_2/Perovskite/Spiro-MeOTAD/Au cell (See Experimental method in chapter4) was put in N_2 environment under continuous illumination of one sun/open circuit state. During 19hour, performance loss was observed: PCE dropped dropped from 18.6% to 13.8% after 19hour. While J_{sc} didn't change much, R_{sh}, V_{oc} dropped from 40Kohm to 20Kohm and from 1.05V to 0.98V, respectively, causing such PCE drop(Fig.2.1.1b). Along with the performance loss, hysteresis type also changed from normal hysteresis to inverted hysteresis (Fig.2.1.1a, b). Such change was reported in device with different perovskite layer, having initial PCE lower than 5%[15]. As in that report, loss of R_{sh} and thus V_{oc}, PCE can be explained by introducing inductance parallel to shunt resistance.

a)

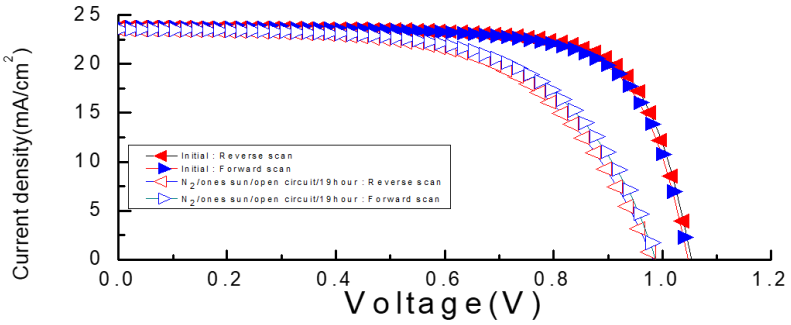

b)

	Direction	J_{sc}(mA/cm^2)	R_{sh}(Kohm)	V_{oc}(V)	R_s(ohm)	FF(%)	PCE(%)
Initial	Reverse	23.7	53	1.05	52.4	74.3	18.6
	Forward	23.8	33.9	1.05	51.7	72.6	18.1
After	Reverse	23.5	14.5	0.981	101	59.8	13.8
	Forward	23.55	20.4	0.987	83.5	61.8	14.4

Figure2.1.1 a) Reverse/forward scanned JV curve for initial state and after 19hour under N_2/one sun/open circuit. b) Table for photovoltaic parameters for reverse/forward scanned JV curve for each initial/final state.

2.1.2. Change in JT curve

To investigate the reason for change in hysteresis type, JT curve was measured. For dramatic comparison, inverted hysteresis device was put longer in same condition. While photocurrent in JT curve for initial/normal hysteresis device is always higher in reverse scan, that of final/inverted hysteresis device is not (Fig.2.1.2.1b, d). Even more, this abnormal JT curve region corresponds to inverted hysteresis region in JV curve (Fig.2.1.2.1c, d, e). Considering voltage sweep also measures transient response, this means that inverted hysteresis is a consequence of abnormal time response.

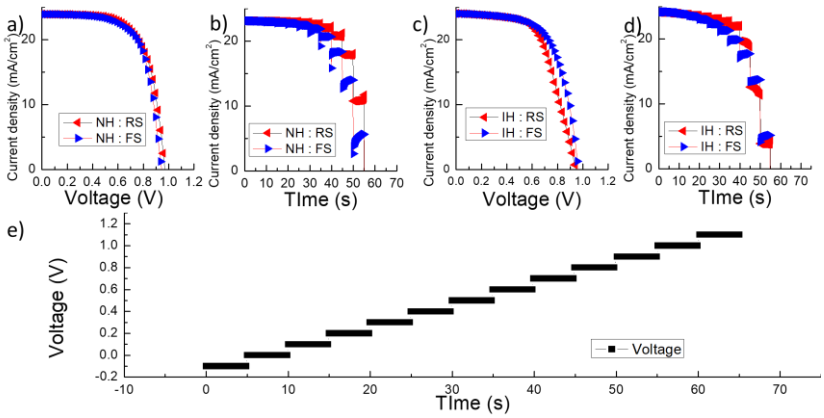

Figure2.1.2.1 a) JV curve and b) JT curve for normal hysteresis device. c) JV curve and d) JT curve for inverted hysteresis device. RS refers to reverse scan, FS refers to forward scan, NH refers to normal hysteresis, and IH refers to inverted hysteresis. e) Time-voltage data for transient response (JT curve) measurement.

For more detailed comparison with abnormal time response and theoretical inductive circuit, JT curve for simpler step voltage input was obtained, with longer range of time. Inverted hysteresis device showed various type of transient response, whereas normal hysteresis device showed only normal transient response (Fig.2.1.2.2a, c, d, e). More than just various type of inequality, crossover of hysteresis type was observed with oscillation (Fig.2.1.2.2d). Assuming that magnitude of inductance depends on DC-bias, just like capacitance does, those are observation of all possible case in suggested RLC circuit (Fig.2.1.2.2b). If capacitive current dominates the transient response, normal transient will be observed (Fig.2.1.2.2a, c). On the other hand, if inductive current dominates the response, abnormal transient will be observed (Fig.2.1.2.2e). In moderate region where those two opposing current-capacitive and inductive-compete each other, oscillation and thus crossover of hysteresis type will be observed (Fig.2.1.2.2e).

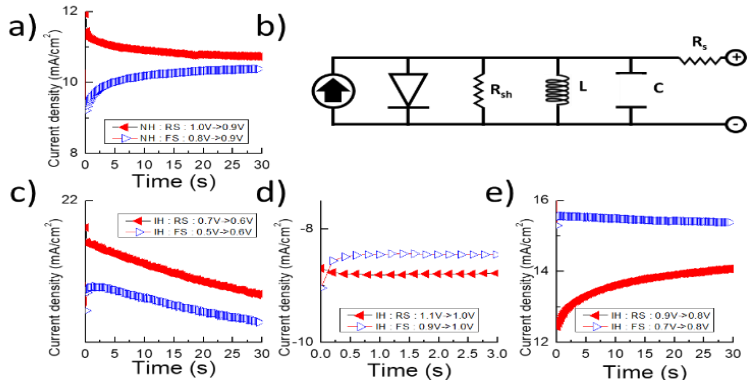

Figure2.1.2.2 JT curve for a) normal hysteresis device to 0.9V. b) equivalent circuit with inductance. JT curve for inverted hysteresis, to c)0.6V, d)1.0V and e)0.8V. Step voltage for transient response analysis were all 0.1V, coming after 30sec for stabilization.

2.1.3. Experimental proof for existence of inductance: EIS

To figure out existence of inductance, EIS measurement was taken. Bode plot of normal hysteresis device shows mono decreasing norm of impedance for increasing frequency, which is theoretically true for RC circuit (Fig.2.1.3a). On the other hand, Bode plot of inverted hysteresis device shows maxima (Fig.2.1.3b, c). This means the existence of inductance parallel to capacitance.

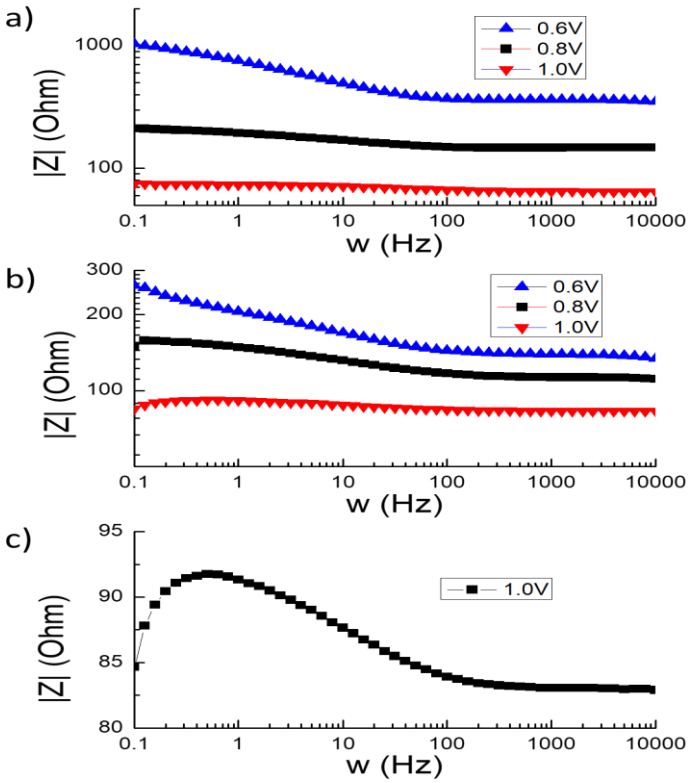

Figure2.1.3 Bode plot of a) normal hysteresis and b) inverted hysteresis device for DC bias of 0.6V, 0.8V and 1.0V. c) Magnified Bode plot in linear scale of inverted hysteresis device under 1.0V DC bias.

2.2. Conclusion

From data above, we can conclude that light/bias (open circuit) induces inductive behavior, resulting abnormal transient response and thus inverted hysteresis. Next question is, of course, is about physical origin of inductance and major factor why it is not observed in initial state and then expressed after light/biased circumstances.

Chapter 3.

Ion channel as an origin of inductance

3.1. Results and discussion

3.1.1. Resemblance to RRAM device

To find out when and why hysteresis type changes, we tested for different light/bias condition. With one sun illumination, such change didn't occur under short circuit(Fig.3.1.1a). After such change occurred, this turned out to be reversible(Fig.3.1.1b). Regarding reversibility as hysteresis without damping, this is similar to mechanism of any memory device.

As an application of perovskite material to memory device, perovskite RRAM device has been reported. Device becomes conductive under bias higher than set voltage, and loses conductivity under bias lower than reset voltage [12, 13, 36]. The device is regarded to be in ON (1) state for higher conductance, and OFF (0) state for lower conductance. To check resemblance in detail, we tested device under periodically repetitive bias condition (1.2V/ -0.2V, one hour for each bias). Result is expressed in terms of hysteresis index($100 * \frac{PCE_{RS}-PCE_{FS}}{PCE_{RS}}(\%)$), which is positive for normal hysteresis device and negative for inverted hysteresis device. The result showed repetitive change in its sign from positive to minus under forward bias of 1.2V and then back to positive again under reverse bias of -0.2V

(Fig.3.1.1c). This means that the phenomena is also of memory effect (in terms of hysteresis index), just like perovskite RRAM device.

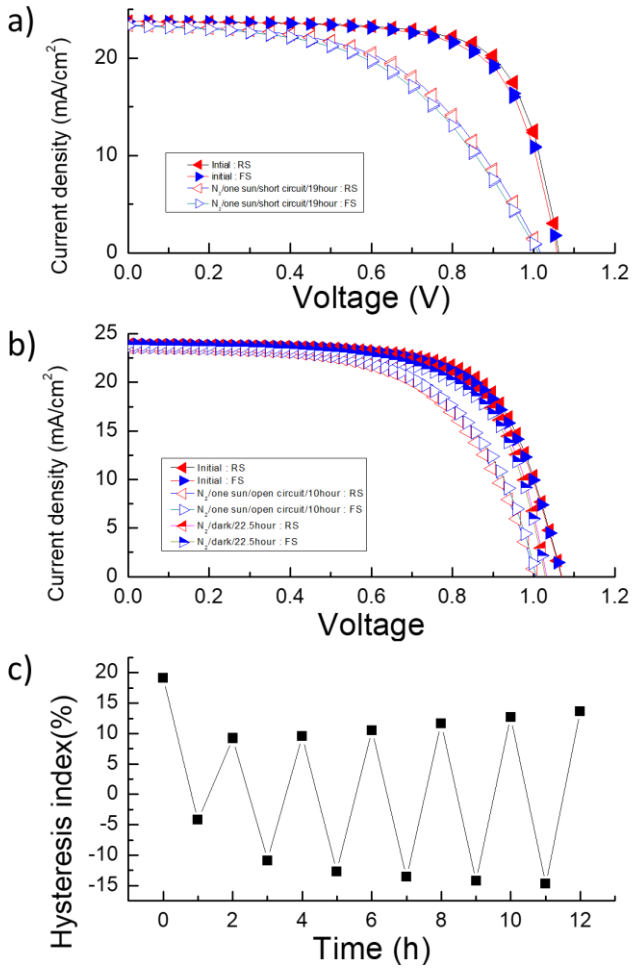

Figure3.1.1 Change in JV curve under a) short circuit case and b) open circuit case and then dark recover. RS/FS refers to reverse/forward scan. c) Result of periodic alternative bias voltage (1.2V, -0.2V. 1hour for each step) in terms of hysteresis index.

3.1.2. Experimental proof for ion channel: HRTEM

Mechanism of perovskite RRAM device is reported to be of formation/deformation of conductive ion channel for ON/OFF state, respectively [12, 13, 36]. To check whether ion channel is present only for inductive device, cross section high resolution transmission electron microscopy(HRTEM) with in-situ energy dispersive spectroscopy(EDS) was conducted for sample prepared via focused ion beam(FIB). Only inverted hysteresis device shows high transmission region (white color) near electron transport layer(SnO_2) (Fig.3.1.2a, b). From EDS analysis, this region turns out to lack halide anion (Iodide: I^-) (Fig.3.1.2c, d). Fast Fourier transform(FFT) image shows low crystallinity in the region, indicating that organic cation (Form-amidinium: FA^+ or Methyl-ammonium:MA^+) which is not detected by EDS analysis may be present in the region. Considering electron transport layer had been connected to cathode (-) during change of hysteresis type, such distribution is energetically reasonable. Right above the region, we could see line shaped high transmission region. Considering high transmission region is iodide deficient, this line shaped region can be regarded as iodide vacancy vertically aligned. Since it is reported that iodide ion and corresponding vacancy forms conductive ion channel [12, 36], we conclude that ion channel is present only in inverted hysteresis device, which shows inductive behavior.

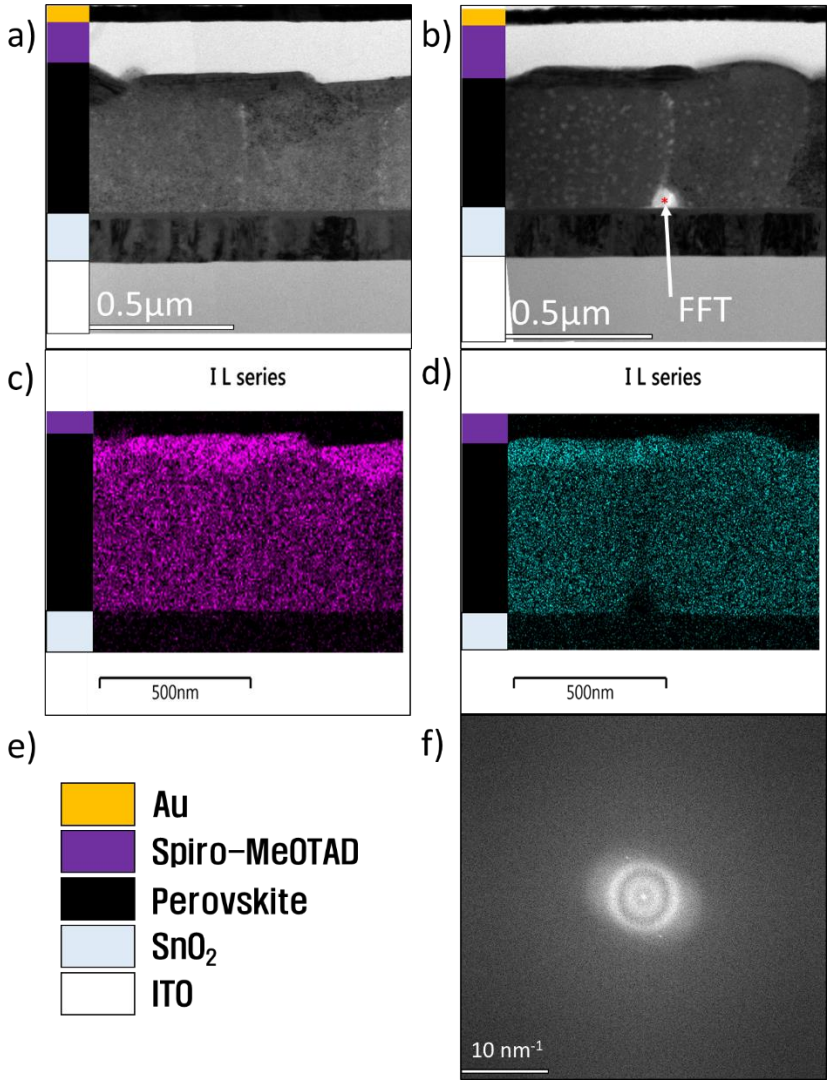

Figure3.1.2 High-resolution TEM image of (a) normal hysteresis device and (b) inverted hysteresis device. Corresponding EDS mapping of iodide atom (L series) of (c) normal hysteresis device and (d) inverted hysteresis device. (e) Fast Fourier transformed micrograph of marked region in (b). Scale bar present in each figure.

3.1.3. How ion channel can act as inductance

Discussion about how ion channel can act as inductance should be done. We suggest that conductive ion channel cause non uniform current density, which induces nonzero magnetic flux (which is canceled to be zero in uniform current density) and thus inductance. Ground loop is good example having inductance due to non uniform current density.

For simple but mathematical explanation, parallel path with different current flow is assumed(Fig.3.1.3). Using basic electromagnetics, we can calculate magnetic flux:

$$\boldsymbol{\phi = \int d\bar{a} \cdot \bar{B} = \frac{\mu d(r-1)}{2\pi} \ln\left(\frac{R+s}{R}\right) I (eq.1)}$$

According to Faraday's law, change in magnetic flux induces induced electromotive force:

$$\boldsymbol{V_{emf} = \frac{d\phi}{dt} = \frac{\mu d(r-1)}{2\pi} \ln\left(\frac{R+s}{R}\right) \frac{dI}{dt} (eq.2)}$$

Since total current is sum of current flow in both path, induced electromotive force can be written as:

$$\boldsymbol{V_{emf} = \frac{\mu d(r-1)}{2\pi(r+1)} \ln\left(\frac{R+s}{R}\right) \frac{dI_{total}}{dt} (eq.3)}$$

Inductance is parameter indicating how much electromotive force is induced for unit change of current over time. Thus, inductance is:

$$\boldsymbol{L = \frac{\mu d(r-1)}{2\pi(r+1)} \ln\left(\frac{R+s}{R}\right) (eq.4)}$$

That way, non uniform current density due to ion channel can act as inductance.

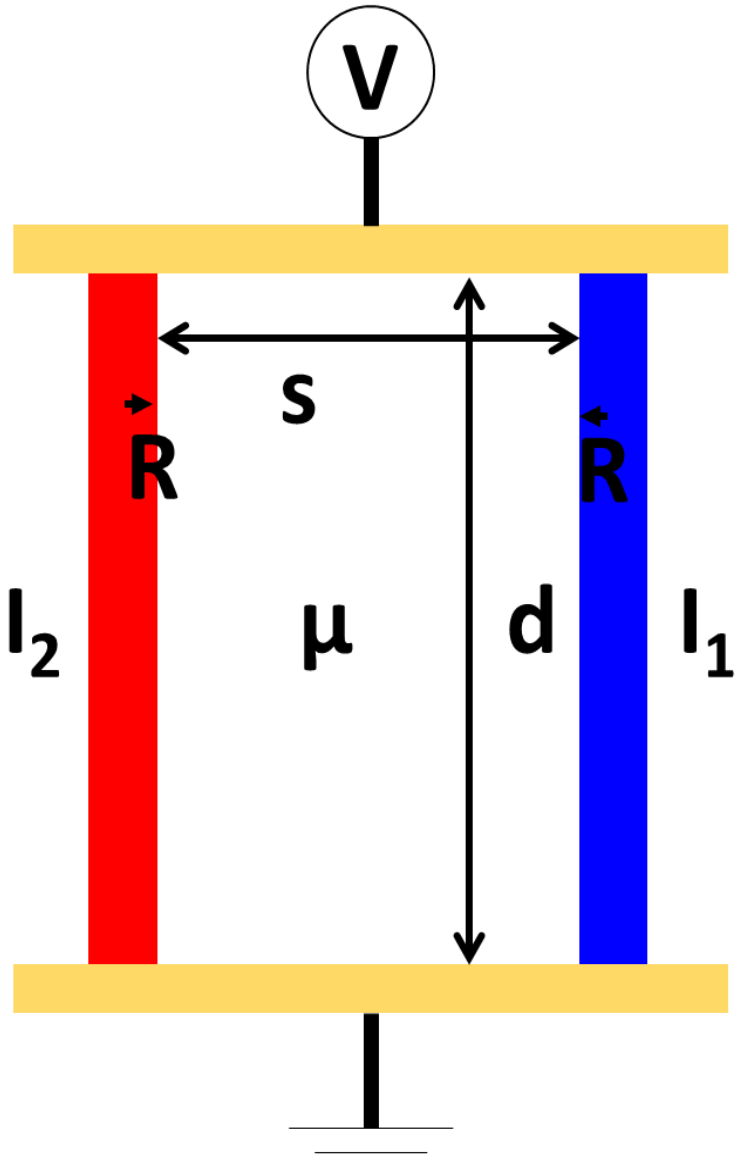

Figure3.1.3 Schematic for explanation how non uniform current density can behave as inductance. Two different current I_1, I_2, length, distance, radius of current path d, s, R, bias voltage V and magnetic permeability μ are shown. Parameter r is ratio of two current I_1 and I_2.

3.2. Conclusion

From data above, we can conclude that ion channel is present in inverted hysteresis device just like in perovskite RRAM device, acting as inductance by forming non uniform current density. With this logic, inductive behavior in other device with presumable non uniform current density, such as mesoporous structured device, device with phase segregation or multidimensional device may be explained.

Chapter 4.

Outro

4.1 Conclusion & future work

Change in hysteresis type from normal hysteresis to inverted hysteresis along with performance loss was reported. Inverted hysteresis here turned out to be consequence of abnormal transient response due to inductance, which was check by EIS. As a physical origin of inductance, we suggested non uniform current density due to ion channel formation in inductive device. Ion channel was observed in inductive device via HRTEM and in-situ EDS. In view of stability problem, composition with easier formation of ion channel should be avoided.

Several questions still remain, leaving potential for future work. First question is about condition for ion channel formation. Being interest in RRAM device application, the answer can also give us criteria for selection of perovskite layer for long term stability. Second question is about fabrication of inductance. Inductance has not been well miniaturized like other components in integrated circuit. This is due to 3 dimensional geometry of inductance. Reported conclusion can be about inductance with 2 dimensional geometry.

4.2 Experimental Methods

4.2.1. Fabrication of perovskite solar cells

As transparent conductive oxide, ITO glass substrates (AMG, 9.5ohm*cm^2, 25*25mm^2) was prepared.

As an electron transport layer, 3%wt SnO_2 colloidal solution was spin coated(4000rpm/30sec) and then annealed (150 degree Celsius/30min).

Perovskite layer was coated in two step method. 600mg PbI_2 was dissolved in 0.95ml DMF/0.05ml DMSO, and then spin coated(2500rpm/30sec). 80mg FAI/8mg MABr/8mg MACl was dissolved in 1ml IPA, and then annealed (130 degree Celsius/30min) after spin coated(5000rpm/30sec).

As a hole transport layer, 72.3mg Spiro-MeOTAD was dissolved in 1ml Chlorobenzene/28.8ul 4-tert-butyl pyridine/17.5ul lithium bis (trifluoromethanesulfonyl) imide solution (520mg lithium bis imide in 1ml acetonitrile) and then spin coated(2000rpm/30sec).

As a metal contact, 50nm gold (Au) was deposited at the rate of 0.3 Å/s by using a vacuum thermal evaporator. All spin coating processes were carried out in a dry room (RH <15%, room temperature).

4.2.2 Characterization(JV/JT curve, EIS and HRTEM)

JV/JT curves were measured by a solar simulator (Oriel Sol3A) calibrated to give one sun using a standard Si photovoltaic cell (Rc-1000-TC-KG5-N, VLSI Standards) with Keithley 2400 Source Meter. Aperture size was 7.29mm^2. Default setting for IV scan was 1.1V to -0.1V/60 point/50ms dwell time.

EIS was conducted using equipment (Metrohm autolab, model : PGSTAT302N)

HRTEM and in situ EDS, FFT were conducted in Korea Advance Nano Fab center (JEM-1000F model from JEOL).

4.3 References

1. Kojima, A., et al., *Organometal halide perovskites as visible-light sensitizers for photovoltaic cells.* Journal of the American Chemical Society, 2009. **131**(17): p. 6050-6051.
2. Kim, H.-S., et al., *Lead iodide perovskite sensitized all-solid-state submicron thin film mesoscopic solar cell with efficiency exceeding 9%.* Scientific reports, 2012. **2**: p. 591.
3. Burschka, J., et al., *Sequential deposition as a route to high-performance perovskite-sensitized solar cells.* Nature, 2013. **499**(7458): p. 316.
4. Jeon, N.J., et al., *Solvent engineering for high-performance inorganic–organic hybrid perovskite solar cells.* Nature materials, 2014. **13**(9): p. 897.
5. Ahn, N., et al., *Highly reproducible perovskite solar cells with average efficiency of 18.3% and best efficiency of 19.7% fabricated via Lewis base adduct of lead (II) iodide.* Journal of the American Chemical Society, 2015. **137**(27): p. 8696-8699.
6. Lee, J.-W., et al., *Tuning molecular interactions for highly reproducible and efficient formamidinium perovskite solar cells via adduct approach.* Journal of the American Chemical Society, 2018. **140**(20): p. 6317-6324.
7. Jung, E.H., et al., *Efficient, stable and scalable perovskite solar cells using poly (3-hexylthiophene).* Nature, 2019. **567**(7749): p. 511.
8. Yuan, M., et al., *Perovskite energy funnels for efficient light-emitting diodes.* Nature nanotechnology, 2016. **11**(10): p. 872.
9. Lin, K., et al., *Perovskite light-emitting diodes with external quantum efficiency exceeding 20 per cent.* Nature, 2018. **562**(7726):

p. 245.

10. Chin, X.Y., et al., *Lead iodide perovskite light-emitting field-effect transistor.* Nature communications, 2015. **6**: p. 7383.
11. Dou, L., et al., *Solution-processed hybrid perovskite photodetectors with high detectivity.* Nature communications, 2014. **5**: p. 5404.
12. Yang, J.M., et al., *1D hexagonal HC (NH2) 2PbI3 for multilevel resistive switching nonvolatile memory.* Advanced Electronic Materials, 2018. **4**(9): p. 1800190.
13. Yoo, E.J., et al., *Resistive switching behavior in organic–inorganic hybrid CH3NH3PbI3− xClx perovskite for resistive random access memory devices.* Advanced Materials, 2015. **27**(40): p. 6170-6175.
14. Guerrero, A., et al., *Properties of contact and bulk impedances in hybrid lead halide perovskite solar cells including inductive loop elements.* The Journal of Physical Chemistry C, 2016. **120**(15): p. 8023-8032.
15. Fabregat-Santiago, F., et al., *Deleterious effect of negative capacitance on the performance of halide perovskite solar cells.* ACS Energy Letters, 2017. **2**(9): p. 2007-2013.
16. Ghahremanirad, E., et al., *Inductive loop in the impedance response of perovskite solar cells explained by surface polarization model.* The journal of physical chemistry letters, 2017. **8**(7): p. 1402-1406.
17. Ebadi, F., et al., *Origin of apparent light-enhanced and negative capacitance in perovskite solar cells.* Nature communications, 2019. **10**(1): p. 1574.
18. Kovalenko, A., et al., *Ionic origin of a negative capacitance in lead halide perovskites.* physica status solidi (RRL)–Rapid Research Letters, 2017. **11**(3): p. 1600418.
19. Unger, E.L., et al., *Hysteresis and transient behavior in current–voltage measurements of hybrid-perovskite absorber solar cells.*

Energy & Environmental Science, 2014. **7**(11): p. 3690-3698.

20. Tress, W., et al., *Understanding the rate-dependent J–V hysteresis, slow time component, and aging in CH 3 NH 3 PbI 3 perovskite solar cells: the role of a compensated electric field.* Energy & Environmental Science, 2015. **8**(3): p. 995-1004.
21. Richardson, G., et al., *Can slow-moving ions explain hysteresis in the current–voltage curves of perovskite solar cells?* Energy & Environmental Science, 2016. **9**(4): p. 1476-1485.
22. Chen, B., et al., *Origin of J–V hysteresis in perovskite solar cells.* The journal of physical chemistry letters, 2016. **7**(5): p. 905-917.
23. Kim, H.-S., et al., *Control of I–V hysteresis in CH3NH3PbI3 perovskite solar cell.* The journal of physical chemistry letters, 2015. **6**(22): p. 4633-4639.
24. Eames, C., et al., *Ionic transport in hybrid lead iodide perovskite solar cells.* Nature communications, 2015. **6**: p. 7497.
25. Sanchez, R.S., et al., *Slow dynamic processes in lead halide perovskite solar cells. Characteristic times and hysteresis.* The journal of physical chemistry letters, 2014. **5**(13): p. 2357-2363.
26. Elbaz, G.A., et al., *Unbalanced hole and electron diffusion in lead bromide perovskites.* Nano letters, 2017. **17**(3): p. 1727-1732.
27. Lopez-Varo, P., et al., *Device physics of hybrid perovskite solar cells: theory and experiment.* Advanced Energy Materials, 2018. **8**(14): p. 1702772.
28. Recart, F. and A. Cuevas, *Application of junction capacitance measurements to the characterization of solar cells.* IEEE transactions on electron devices, 2006. **53**(3): p. 442-448.
29. Almora, O., et al., *Noncapacitive hysteresis in perovskite solar cells at room temperature.* ACS Energy Letters, 2016. **1**(1): p. 209-215.
30. Tress, W., et al., *Inverted current–voltage hysteresis in mixed*

perovskite solar cells: polarization, energy barriers, and defect recombination. Advanced Energy Materials, 2016. **6**(19): p. 1600396.

31. Nemnes, G.A., et al., *Normal and inverted hysteresis in perovskite solar cells.* The Journal of Physical Chemistry C, 2017. **121**(21): p. 11207-11214.
32. Sepalage, G.A., et al., *Copper (I) iodide as hole-conductor in planar perovskite solar cells: probing the origin of J–V hysteresis.* Advanced Functional Materials, 2015. **25**(35): p. 5650-5661.
33. Shen, H., et al., *Inverted hysteresis in CH3NH3PbI3 solar cells: role of stoichiometry and band alignment.* The journal of physical chemistry letters, 2017. **8**(12): p. 2672-2680.
34. Cojocaru, L., et al., *Simulation of current–voltage curves for inverted planar structure perovskite solar cells using equivalent circuit model with inductance.* Applied Physics Express, 2017. **10**(2): p. 025701.
35. Ahn, N., et al., *Trapped charge-driven degradation of perovskite solar cells.* Nature communications, 2016. **7**: p. 13422.
36. Kwon, D.-H., et al., *Atomic structure of conducting nanofilaments in TiO 2 resistive switching memory.* Nature nanotechnology, 2010. **5**(2): p. 148.

페로브스카이트 태양전지 내부 이온채널에 기인한 인덕턴스

정 기 완
기계항공공학부
공과 대학원
서울대학교

초록

페로브스카이트 태양전지의 인덕티브 루프(혹은 음의 축전기 성분) 의 원인으로써 실제 인덕턴스를 제안하였다. 광/전압에 의한 인덕티브 루프, 이상과도현상 그리고 역전된 히스테리시스가 모두 광/전압에 의한 인덕턴스에 의한 것임을 주장하였다. 인덕턴스성분이 이온 채널에 의한 비균일 전류밀도 에 의한 것임을 제안하였으며, HRTEM 측정과 EDS 측정을 통해 역전된 히스테리시스를 보이는 소자에서 이온 채널이 존재함을 보였다.

주요어:

페로브스카이트 태양전지 **역전된 히스테리시스**

인덕티브 루프 **음의 축전기** **이온 채널**

학번: 2017-22307

감사의 글

기계공학 학사를 따고서, 태양전지에 대하여 아무것도 모른 채 연구를 시작하게 됐던 제가 기억납니다. 새로운 지식을 습득하고자 내린 스스로의 선택이었으나, 그 긴 시간 동안 공부할 수 있었던 것은 기다려 주신 저의 지도 교수님, 최만수 교수님 덕분이라고 믿습니다. 세계적 수준의 장비로 연구할 수 있었던 점, 늘 연구적인 메시지를 남겨주신 점, 그리고 학자로서의 집념은 어때야 하는지를 보여주신 점 깊이 감사드리며, 덕분에 저의 학위에 걸맞는 지식과 자질을 갖추게 되었습니다.

가까이에서 저와 사수/부사수 관계로 저를 지도해주신 안남영 박사님께도 감사의 말씀을 드립니다. 박사님을 닮고싶어 질문을 던지는 과정에서도 많이 성장했고, 그 과정에서 직접 조언해주신 내용들은 정말 큰 귀감이 되었습니다.

연구실 생활함에 있어 여러모로 조언해 주신 선배님들께도 감사드립니다. 연구실을 떠나신 곽귀성 박사님, 김민철 박사님, 윤정진 박사님, 장세근 박사님 뿐 아니라 아직 연구실에 계신 이건희 박사님, 윤희태 선배님, 신성수 선배님, 홍승찬 선배님, 변준섭 선배님, 박민철 선배님 감사드립니다.

비슷한 시기에 들어와 같이 배우며 같이 고생한 언수형, 연우형, 지우, 기준이형, 준형이형, 민성이형, 성성이, 주연이, 같이 시간쓰며 즐거운 일들이 있어 힘내서 연구할 수 있었습니다.

다사다난했던 학창시절, 음악이 하고싶던 제가 이정도 교육을 받을수 있도록 지금까지 지도해주시고 지원해주시고 응원해주신 부모님과 형님. 감사드리며, 사회와 가정에 꼭 필요한 존재가 되어 자랑스레 해드리겠습니다.

끝으로, 이 학위논문을 읽어주시는 모든 분들께 감사드립니다. 이 논문을 읽음으로써, 여러분은 제가 석사학위동안 만든 결론들을 의미있게 만들어 주셨습니다. 앞으로의 연구 또한 누군가에게 읽혀질것이라 기대하며 더 좋은 연구 하도록 하겠습니다.